Journal of Cluster Science (2023) 34:1087–1098
https://doi.org/10.1007/s10876-022-02292-9

ORIGINAL PAPER

Platinum as a Novel Nanoparticle for Wound Healing Model in *Drosophila melanogaster*

Janmejaya Bag[1] · Sumit Mukherjee[1] · Manamohan Tripathy[2] · Rudramadhab Mohanty[1] · Pranab Kumar Shendha[1] · Garudadhwaj Hota[2] · Monalisa Mishra[1]

Received: 19 February 2022 / Accepted: 24 May 2022 / Published online: 14 June 2022

Abstract

Platinum nanoparticles (PtNPs) are widely used as a potent antioxidant and thus, have gained interest in the field of biomedical research. The present study depicted the non-cytotoxic and non-genotoxic properties of PtNPs using *Drosophila melanogaster* as in vivo model system. The PtNPs are proposed to be used for wound healing in *Drosophila*. PtNPs were found to quench the reactive oxygen species (ROS) by interacting with the antioxidant enzymes, such as superoxide dismutase, catalase, and glutathione peroxidase. The application of the PtNPs on the wound site showed a tremendous healing potential reported for the first time. The wound was healed within a short period of time as compared to the untreated wound. A comparative study of mitochondrial staining and mitochondrial protein measurement revealed that PtNPs help in scavenging the internal ROS and enhance the mitochondrial function. PtNP showed a negligible cytotoxic effect and no genotoxic effect. This finding can lead to the future applications of PtNPs in nanomedicine.

Graphical Abstract

Platinum nanoparticles help in scavenging the reactive oxygen species and act as a nano-antioxidant. It also induces mitochondrial function and increases the mitochondrial protein and copy number. Platinum interacts with the hemocytes without any toxic effect on the cells. PtNPs significantly induced the wound healing process to be completed in a short time.

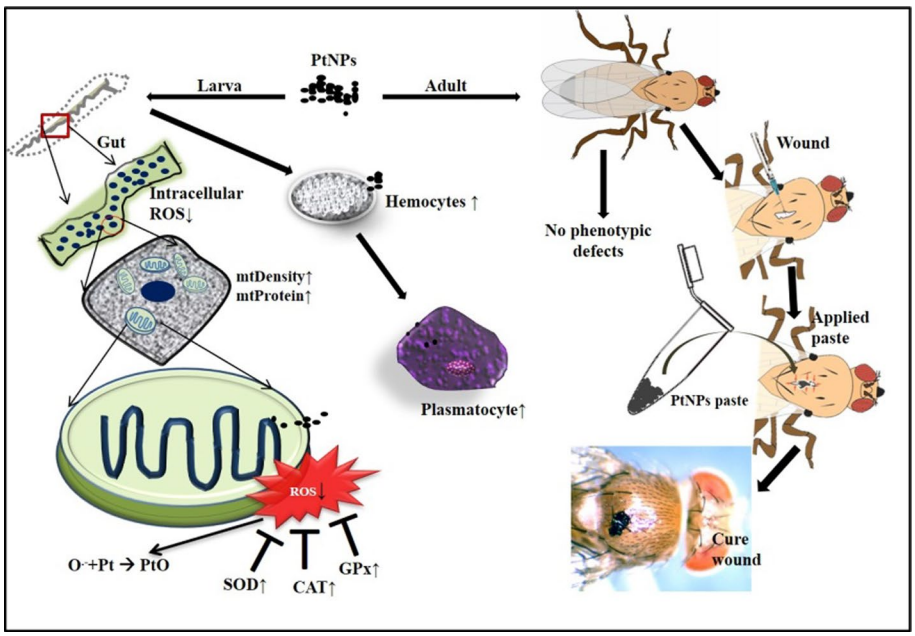

Keywords Platinum nanoparticle · ROS · Wound healing · Angiogenesis · *Drosophila melanogaster*

Extended author information available on the last page of the article

Introduction

Nanotechnology is one of the emerging fields of modern science which include the development of a number of nanomaterials, including nanoparticles (NPs) possessing unique physicochemical and optoelectronic properties, to be used in several applications. Metallic NPs such as titanium, silver, and platinum are used extensively to fuel the cells, as biosensors in biomedical industries, petrochemical industries, photonics, electronics, organic catalyst, pharmaceuticals, and automobiles [1–4]. Among the metallic NPs, platinum nanoparticles (PtNPs) have been widely used as a potential catalyst due to their high conductance and reactivity [5]. PtNPs have also been seen to have a protective role against reactive oxygen species [6–9]. It was also reported that PtNPs do not show any cytotoxic and genotoxic effects in in vitro studies of different cell lines such as HeLa [10, 11], HepG2, MI-38, TIG-1, and MRC-5 [12–14]. However, some studies also reported that cellular uptake of PtNPs shows duration, size, and dose-dependent cytotoxic effects [15, 16]. Moreover, in a selective way, PtNPs have been shown to induce the breakdown of DNA strands in human colon cancer cell lines after the cellular uptake of NPs and solubilized inside the nucleus [14, 17]. Further investigation of PtNPs showed that they can be used in wound healing and therapeutic agents along with the other noble nanoparticles due to their improving antioxidant defense mechanism [10, 18, 19]. Superoxide dismutase (SOD) plays the first line of defense mechanism that oxidizes the superoxide radicals into hydrogen peroxide, followed by catalase and glutathione peroxidase enzymes that help in the breakdown of hydrogen peroxide to water and oxygen molecule [20, 21].

Noble nanoparticles such as gold and palladium are often used along with PtNPs [10, 19]. These NPs show strong catalytic activities e.g., oxidation, hydration, and hydrogenation reactions [22, 23]. Platinum and palladium nanoparticles are used for studying aging-related skin atrophy in mice models [10]. Over 100 years ago in 1915, Dr. H. Naguchi and Dr. S. Ishizuka formulated an idea for creating a paste of palladium and platinum NPs solution and named it as PAPLAL [10, 24]. PAPLAL has been used in the treatment of Japanese patients having hives, burns, gastric ulcers, lung inflammation, frostbite, and rheumatoid arthritis [24]. PtNPs can further increase the concentration of Pt in a treatment cell as compared to the control cells [25]. Sakaue et al. also reported that, when *C. elegans* were treated with PtNPs, the internalized concentration of Pt increases tremendously in the nematodes [26]. All of these results showed that PtNPs taken by the cells inhibit the oxidative stress by inhibiting the internal ROS and help in wound healing [10]. Many reports were available regarding the toxic and nontoxic effects of PtNPs; however, the authors were unable to suggest the other appropriate aspect uses of PtNPs. There are only a few reports available regarding the relationship between the PtNPs, ROS, and mitochondria biogenesis. Therefore, in this report, we have studied the various parameters related to antioxidant enzymes and mitochondria biogenesis. PtNPs were introduced as a new application to help the wound for rapid healing.

Drosophila melanogaster is used as a promising model organism to study the toxicity of different NPs [27–30]. The model possesses, 1) a small number of chromosomes i.e., four pairs, it shares 75% of the human disease genome, 2) it is easy to maintain and manipulate, and 3) many generations can be studied in a short period because its life span is about 30–45 days, 4) all the genetic tools are available. All these assets make it an ideal model organism to study various aspects of nanoparticle treatment. Our current study checked the cytotoxic and genotoxic effects of PtNPs using *D. melanogaster*. After checking the biocompatability, the wound healing potential of PtNPs was checked in *D. melanogaster*. This is the first study report of PtNPs on *D. melanogaster* in accordance with the in vivo models such as *C. elegans* and mice.

Material and Methods

Materials

Hexachloroplatinic acid (H_2PtCl_6) and Polyvinylpyrrolidone (PVP) were purchased from Sigma-Aldrich. The chemicals for anti-oxidant assays such as Bovine serum albumin (BSA), L-methionine, Hydroxylamine hydrochloride, Folin & Ciocalteu's phenol reagent, Ethylenediaminetetraacetic acid, Copper sulfate solution, Sodium potassium tartrate, Riboflavin, disodium hydrogen phosphate, 5,5'-dithiobis-(2-nitrobenzoic acid), Sulphanilamide N-1-Naphthylethylenediamine dihydrochloride, Orthophosphoric acid, Reduced glutathione, Sodium azide, Hydrogen peroxide, Trichloroacetic acid, 2,2-Diphenyl-1-picrylhydrazyl Methanol, and ascorbic acid were purchased from HiMedia Pvt. Ltd, India. Phenylmethylsulfonyl fluoride (PMSF) was procured from ThermoFisher Scientific, India. All the mentioned chemicals were of molecular and analytical grade and used without any modifications.

Synthesis of Platinum Nanoparticle (PtNPs)

PtNPs were synthesized by an earlier reported method with slight modifications [31]. In a typical synthetic approach, equal proportion of H_2PtCl_6 and PVP (1:1 wt. ratio) were mixed into 60 mL of distilled water and stirred vigorously on a magnetic stirrer to form a homogeneous orange-yellowish solution. The obtained solution was transferred to a 100 mL Teflon-lined stainless-steel autoclave and heated subsequently at 160 °C under autogenous pressure for 8 h. After the reaction was completed, the autoclave was cooled down to room temperature. The acquired dark grey colored precipitate was then rinsed and centrifuged with distilled water before being dried in a hot air oven at 60 ºC for 24 h. The obtained powder was suitably grounded using a pestle and mortar and labeled as PtNPs.

Characterization of Nanoparticle

The nanostructures of the PtNPs were characterized by X-ray diffraction (XRD, XRDPHILIPS PW 1830, Japan), field emission scanning electron microscopy (FESEM/EDX, FEI NovaNano SEM 450, Japan), Attenuated total reflectance Fourier transforms infrared spectroscopy (alpha ATR-FTIR, Bruker), DLS and Zeta potential (Zetasizer Malvern NANO-ZS-90, UK).

Fly Rearing

D. melanogaster (*Oregon-R+*) wild-type flies were obtained from the C-CAMP fly facility, Bangalore, India. *UAS-mCD8GFP* flies were from the Center for Human Genetics, Bengaluru. The female and male flies were transferred to each vial in an 8:5 ratio respectively. The flies were kept at 25 °C constant temperature and 70% humidity for 12 h of light and dark conditions. For the toxicity study, PtNPs were added to the fly food to achieve the concentrations of 50, 100, 200, and 400 µg/mL. The treatment of doses was selected from LD50 values of PtNPs measured from in vitro and in vivo studies.

Evaluation of Non-cytotoxic Potential of PtNPs

The PtNPs-fed larval gut was dissected and co-stained with DAPI and DCFH-DA to check the effect of PtNPs on the gut by following Priyadarshini et al., [32]. A detailed method is given in the supplementary section. DAPI stains the nuclei and DCFH-DA stains the ROS generated from the mitochondria. The number of fragmented nuclei was counted and plotted for each concentration. The intensity of DCFH-DA was also plotted for each concentration to know the cellular stress generated after PtNPs treatment. The gut was also stained with trypan blue by following Bag et al. [2], to check if there is any membrane damage due to PtNPs treatment.

Measurement of Oxidative Stress After PtNPs Treatment

Late 3rd instar larval hemolymph was used to check the oxidative stress. Briefly, 25 numbers of third instar larvae were collected. The larvae were pricked carefully near the thoracic region by keeping on an icebox to prevent melanization. Larvae were centrifuged at 4500 rpm for 10 min at 4ºC. 10 µL of the hemolymph was collected in a 1.5 mL eppendorf tube. To the tube, an equal amount of 1X phosphate buffered saline (PBS) was added. The hemolymph was used for the NBT assay by following Nayak et al., 2019 and Bag et al. 2020 [33, 34]. Briefly, to the hemolymph equal volume of NBT (1.6 mM) solution was added and left for 1 h in dark. After 1 h, an equal volume of 100% glacial acetic acid (GAA) was added and incubated for 5 min to stop the reaction. Then 150 µL of 50% GAA was added and measured the absorbance at 595 nm in a microplate reader (Elisa Biobase, EL10A). A similar procedure was followed for the measurement of oxidative stress on adult flies in a time-dependent manner. Adult flies were taken from alternative days for the analysis of oxidative stress (i.e., after hatching of 2, 4, 6, 8, and 10 days young flies). Other antioxidant enzymes like SOD, catalase, and glutathione peroxidase (GPx) are also measured (S2).

Number of Mitochondria Within the Gut

This study is crucial for the detection of the percentage of mitochondria inside the cells. For this, Alsford et al., 's staining procedure was followed [35]. Briefly, third instar larval and adult (6–8 days young flies) guts were isolated and fixed in 4% paraformaldehyde (PFA) at 4 °C. Then, the guts were taken out from PFA and washed with 1X PBS twice. Then to permeabilize the gut 4% BSA-PBST was used twice for 10 min each. After that, the guts were stained with Mito-Tracker™ Red CMXRos (100 nm, Invitrogen, M7512 Molecular Probes) for 10 min, washed with 1X PBS once, and counterstained with DAPI (1 µM) for 5 min to visualize DNA. After that, the guts were mounted on a grease-free slide with 20% glycerol and covered with a coverslip. Then the slides were observed under the fluorescence microscope (Olympus BX50, Japan).

Quantification of Mitochondrial Protein

Mitochondrial protein quantity was measured by following the Dhar et al. and Brandt et al. method [36, 37]. Briefly, thirty adult (6–8 days old) flies were taken and freezed for 10 min to stop their metabolism. The flies were homogenized with 2 ml of mitochondrial isolation buffer (MIB) at 4 °C (pH 7.2) containing 1 mM EGTA, 20 mM Tris–HCl, and 310 mM sucrose. This homogenate was filtered with a 100-µm nylon mesh filter and the filtrate was centrifuged at

800 g for 10 min at 4 °C. The supernatant was centrifuged at 4500×*g* for 15 min at 4 °C to pellet out the mitochondria. The pellet was suspended in 100 µL of MIB. The mitochondrial protein concentration was determined by the Lowry et al., method taking BSA as a standard [38].

Hemolymph and Pt–NPs Interaction

The hemolymph and PtNPs interaction study were done by taking *UAS-mCD8GFP* larvae. Briefly, ten 3rd instar larvae were taken and washed with 1X PBS. The larvae were pricked with a fine needle in the thoracic region in an eppendorf tube on an icebox. Hemolymph was collected by centrifugation at 8000 rpm (4 °C) for 10 min. Then, 10 µg/mL concentrations of PtNPs were added to the 5 µL of hemolymph. A short spin for 2 min was given to settle down the hemocytes and allow the nanoparticles to mix well with the hemolymph. A smear was made by taking the hemolymph on a grease-free slide and drying it for 5 min. The images were taken in a fluorescence and bright field microscope (S3). For the study of SEM and EDX analysis of PtNPs interaction, the protocol by Bag et al., 2020 was followed [39], The isolated hemolymph was spread over a slide of 1 cm^2. Then fixed with absolute methanol and dried for 48 h in an oven. The slides were coated with gold and images were taken in SEM (Nova NanoSEM 450).

Phenotype

The adult phenotype was monitored by screening the eye, wing, bristle, and head of 50 adult flies (3–4 days old). The images were taken with the help of a USB Digital Microscope (S2 USB 8 Led 1X-500X, Generic). From the adult phenotypic analysis, it was shown that there were no defects in the eye, bristle, and wings. This confirmed that, PtNPs is non-genotoxic to the organism at appropriate concentration.

PtNPs for Wound Healing

A wound-healing experiment was performed by making a paste of PtNPs and applied on the surface of the wound. Briefly, an adult 4–5 days old fly (N = 20) was taken and anesthetized with diethyl ether for 30 s. After that, flies were placed on a petriplate with the help of sticky gum. The petriplate was put under the stereo zoom microscope and the recording was started. By focusing the thoracic region in 100X magnification, a small cut was made with the help of an insulin needle (31 gauge × 15/64, Hindustan Syringes & Medical Devices Ltd, India) to develop a wound (Approx. area > 0.06 mm^2). After the wound was developed, a little pinch (≈1/100th mg) of PtNPs paste (1 mg in 10 µL of miliQ water) was applied to the wounded surface with the help of an insulin needle. Then, the fly was left till the wound was completely healed. The time taken for the wound to heal was noted and compared between the PtNPs treatment and without treatment.

Wound Healing Analysis

Wound healing analysis was done by comparing the treated with the non-treated control group. The process of wound healing was recorded under a confocal microscope (Leica, SP8). The videos were processed in ImageJ software and the actin filaments movement was measured, by staining the wound with phalloidin congugated red fluorescence dye. From the videos, the kymograph was plotted with respect to the actin movement events.

Wound Closure Analysis

The wound closure rate was measured by tracing the wound on different time points, such as 1, 30, 60, 90, 120, 150, 180, and 360 min using the stereo zoom microscope images and videos were processed on ImageJ measurement software. The wound of control and PtNPs treatment was measured from fifteen numbers of adult flies till the wound get totally healed. Changes in the wound area were evaluated by an indication of the rate of wound healed or the wound contraction with respect to time. The evaluated surface area was used to calculate the percentage of wound closure by taking the initial size of the wound as 100 percent, and calculated from the formula [40, 41];

$$\%\ \text{of wound closure} = \frac{(\text{wound area on 1 min} - \text{wound area on} \times \text{minutes})}{\text{wound area on 1 min}} \times 100$$

where x is times in minutes (i.e. 30, 60, ……., and 360).

Statistical Analysis

All the experimental data were analyzed in GraphPad Prism 5.0 software. XRD and FTIR data graphs were obtained by using X'Pert HighScore graph software and OriginPro 2020b graph software respectively. Kymograph was obtained from ImageJ software. The data are interpreted by Mean ± SEM values with the significance $^{*}P < 0.05$, $^{**}P < 0.01$, $^{***}P < 0.001$ by unpaired two-tailed student t-test.

Results

Characterization of Nanoparticle

Figure 1a shows the XRD pattern of PtNPs, which shows two prominent peaks at 39.8° and 46.3° specifying the (111)

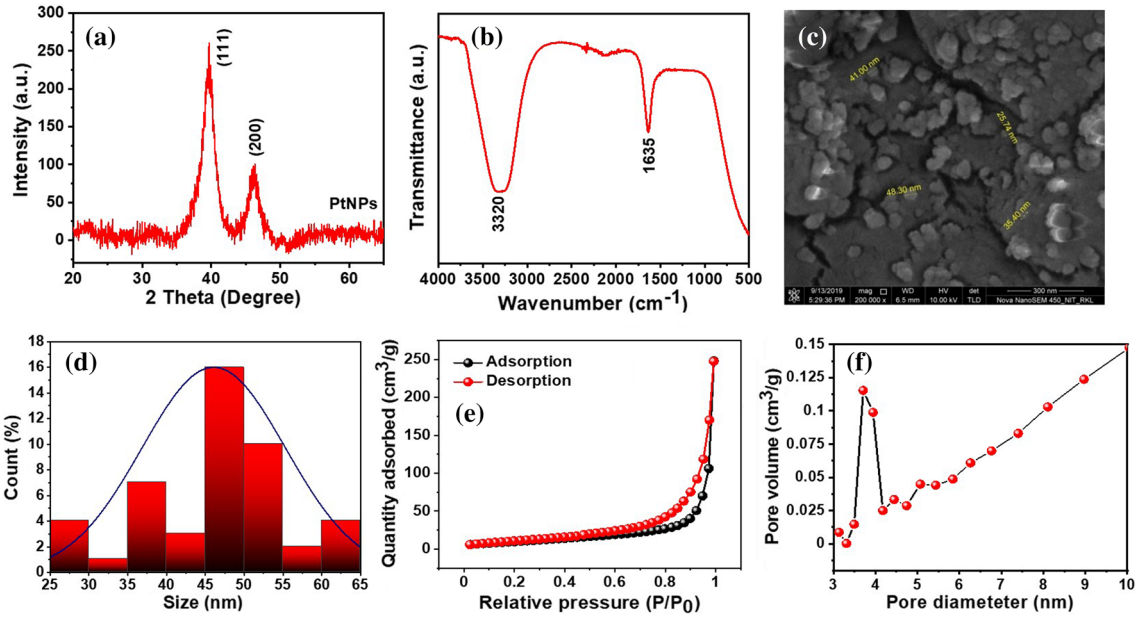

Fig. 1 Characterization of PtNPs, **a** XRD analysis, **b** FTIR analysis, **c** FESEM analysis, **d** distribution curve from FESEM analysis, **e** and **f** BET-analysis

and (200) planes of face-centered cubic (fcc) lattice confirms the successful formation of PtNPs [31, 42]. Figure 1b indicates the FTIR spectra of PtNPs. The broadest IR spectrum measured at 3320 cm^{-1} is due to the stretching vibrations of hydroxyl groups. Furthermore, the intense band at 1635 cm^{-1} was attributed to the C = O stretching vibration of PVP residue present in the sample [43, 44]. The morphology and size distribution of the PtNPs was evaluated by FESEM analysis (Fig. 1 c & d). Ultra-small spherical PtNPs with an average diameter of 45–50 nm were observed. Again, the average size of PtNPs was measured by dynamic light scattering (DLS) (Fig. S1 a). It was found that the average size of the PtNPs was about 100 nm, which is comparatively greater than that determined by FESEM, which is due to the aggregated behavior of the suspended particles. Furthermore, the Zeta-potential of the PtNPs at neutral pH was found to be -36.5 eV (Fig. S1 b). The N_2 adsorption–desorption isotherm was used to determine the specific surface area and pore size of PtNPs, as shown in Fig. 1 (e & f). The acquired data reveal that the produced PtNPs have a type III adsorption isotherm with a specific surface area of 33.0 m^2/g, indicating that they are nonporous. PtNPs have a pore size of 3.708 nm and a pore volume of 0.39 cm^3/g, according to the BJH pore size distribution curve.

Evaluation of Non-cytotoxic Property of PtNPs

Nanoparticles fed to the flies pass through the gut and come in direct contact with the gut epithelial cells. To check whether the NPs induce any cell damage, the cytotoxicity of these cells was checked. DAPI is used to detect DNA damage after exposure of the cells to any toxic compound. The percentage of DNA damage observed was insignificant in the lower concentration of PtNPs treatment (Fig. 2a-e). The percentage of DNA breakdowns in the control and treatment groups were represented in the graph (Fig. 2m). From the internal gut staining of the larva by DCFH-DA, it was observed that PtNPs can reduce the internal ROS activities (Fig. 2f-j). The total fluorescence of the internal gut cell was plotted on the graph (Fig. 2n). This finding was supported by the NBT assay as well as the increased level of anti-oxidative enzymes, suggesting PtNPs help in the reduction of ROS and protect the cells from oxidative stress. This result was similar towards the finding of antioxidant mimic of other reports given by many researchers [8–11].

Intracellular ROS Level

To measure the amount of intracellular ROS, and NBT assay was performed in the third instar larval hemolymph. From the NBT assay, it was found that the formation of ROS reduced significantly in the PtNPs treated group as compared to the control (Fig. 3a). From the adult hemolymph NBT assay, it was observed that the amount of ROS was higher at the initial adult stages. On day 4 of ROS analysis, it was observed that the highest amount of ROS produced by the cells as platinum NPs were marked as foreign particles for the cells. From 6 day onwards young flies show a remarkable reduction of ROS levels as compared to the control flies (Fig. 3b). Thus, the NBT assay suggests that

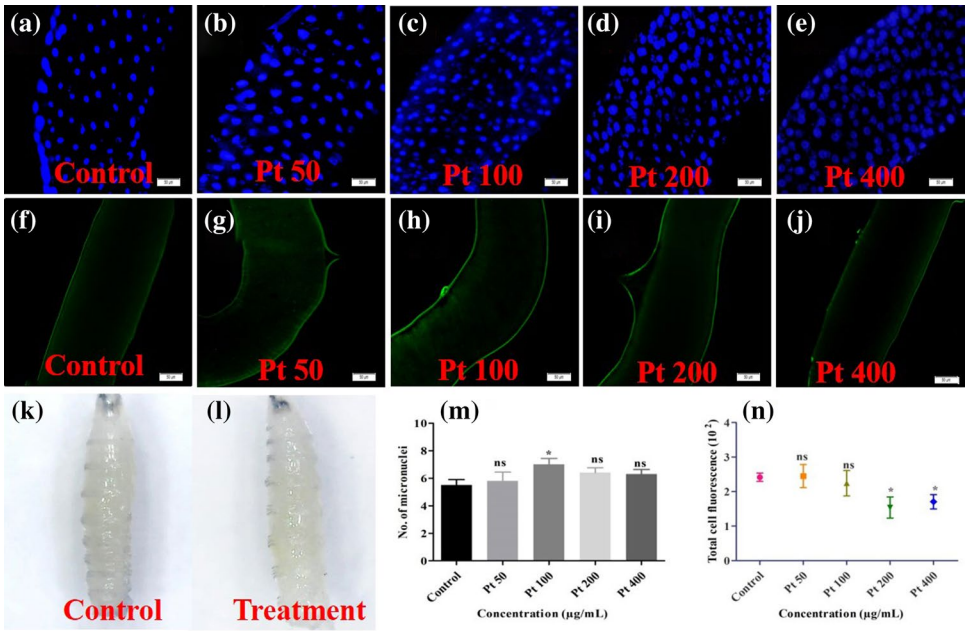

Fig. 2 Histological staining of the larval gut; **a**–**e** DAPI staining of the gut of control and PtNP treated groups; **f**–**j** DCFH-DA staining of the gut of control and PtNP treated groups; **k** trypan blue staining of control larva; **l** trypan blue staining of treated (400 µg/mL PtNP); **m** the percentage of a fragmented nucleus from DAPI staining; n) total cell fluorescence of internal gut from DCFH-DA staining. *ns* non-significant, *indicates $P < 0.05$

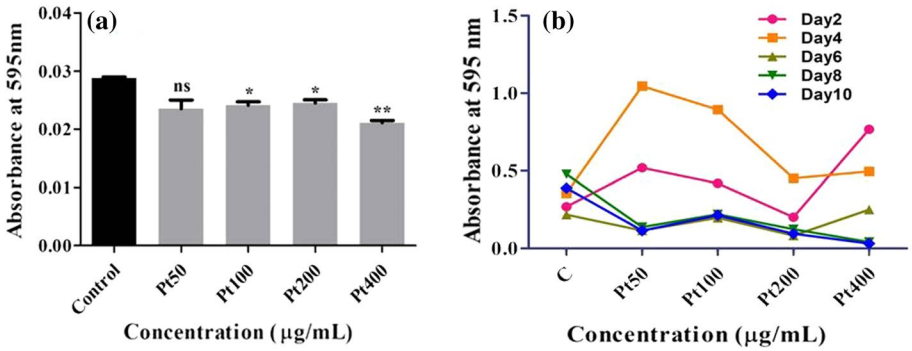

Fig. 3 Measurement of ROS by NBT assay; **a** 3rd instar larval hemolymph; **b** days dependent adult hemolymph. *ns* non-significant, *indicates $P < 0.05$, **indicates $P < 0.01$

the PtNPs play a vital role in the scavenging of ROS. The formation of ROS was seen in the gut, where DCFH-DA staining of the gut epithelial cells showed reduced total cell fluorescence of the PtNPs treated larval gut, indicating less ROS as compared to the control (Fig. 2n).

Measurement of Mitochondrial Number and the Protein Content

Mitochondria are the power pack of the cell and are involved in many cellular mechanisms including oxidative stress pathways. Following a significant reduction in ROS amount and elevated level of anti-oxidative enzymes, we sought to check mitochondria localization within the gut using Mito-tracker staining (Fig. 4a). The mitochondrial protein was also quantified in the control and PtNPs treated gut (Fig. 4b). In PtNPs treated gut, enhanced mitochondrial proteins were detected. Mito-tracker staining (CMXRos) of PtNPs treated gut also revealed a greater number of mitochondria within the gut of 400 µg/mL gut as compared to the non-treated control (Fig. 4a). It was due to the initial increased amount of ROS level that triggered more number of mitochondria to be produced to overcome the oxidative stress. Later on, these cells were acquainted with PtNPs and stayed healthy because PtNPs do not cause any affect or damage to mitochondria. Hence, PtNPs act as an antioxidant to the cells and help in scavenging the ROS and defense from oxidative stress, which was observed from antioxidant measurements (Fig. S2). The number of mitochondria presented per slide in an area of 1 cm^2 was quantified and plotted in the graph (Fig. 4c).

PtNPs Show Nontoxicity to the Hemolymph

It was crucial to check the interaction of hemolymph and PtNPs before studying its application. From the interaction study of PtNPs-hemolymph, no membrane damage and cell damage were found (Fig. 5a-e). From the treatment, the EDX analysis reveals the abundance of three ions i.e., Ca^{+2}, Mg^{2+}, and Na^{+} as 16.61%, 9.30%, and 25.84% respectively

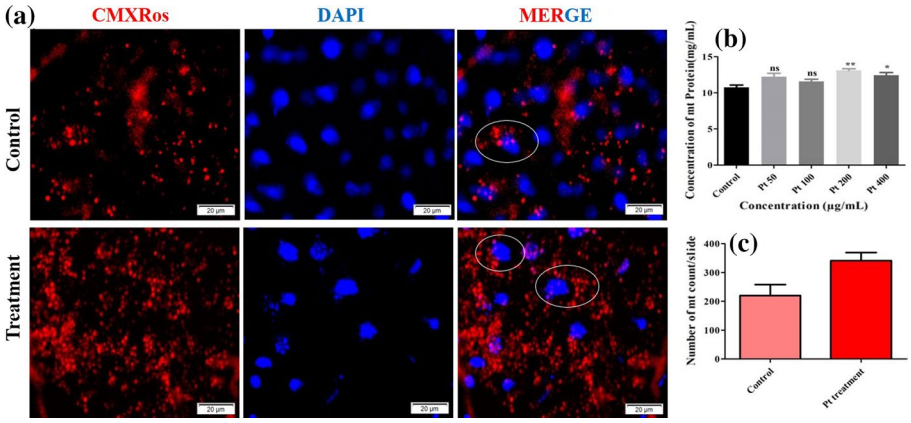

Fig. 4 Mito-tracker CMXRos red staining of the larval gut; **a** counterstaining of CMXRos (Mitochondria, Red color), DAPI (Nucleus, Blue color); **b** mitochondrial protein quantification; **c** graphical representation of the number of mitochondria count from a slide of area 1 cm^2

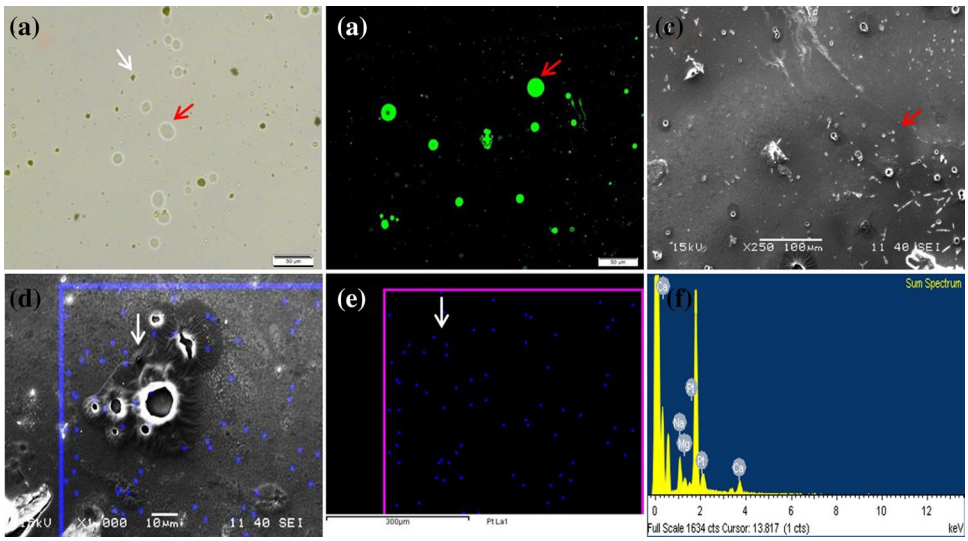

Fig. 5 Interaction of PtNP and hemocytes; **a** bright-field image of hemocytes and PtNPs; **b** fluorescence image of hemocytes showing no membrane damage; **c** SEM image of hemocytes and PtNP; **d** interaction of single hemocytes with PtNP; **e** presence of applied Pt-NP on hemolymph (blue color); **f** EDX elements analysis of hemolymph. (White arrow showing PtNPs and Red arrow showing hemocytes)

(Fig. 5f). Quantification of different types of hemocytes after PtNPs treatment are given in S3.

Phenotype Analysis of Flies Hatched After PtNPs Treatment

The adult phenotype was monitored by screening the eye, wing, bristle, and head of 50 adult flies (3–4 days old). The images were taken with the help of a USB stereo zoom camera. From the adult phenotypic analysis, it was shown that there were no defects on the eye, bristle, and wings in any concentrations (Fig. 6).

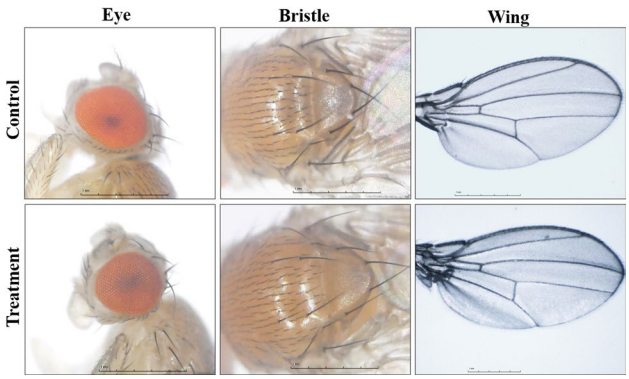

Fig. 6 Phenotypic analysis of adult flies i.e., eyes, bristles, and wings showed non defect on treatment with PtNP

PtNPs Promote Wound Healing in Adult Flies

The wound healing and regeneration of tissue were effectively studied in a wound healing model of *Drosophila* and found that applying PtNPs on the site of the wound enhances tissue growth and angiogenesis. As a result, the tissues at the site of PtNPs administration grow and heal faster as compared to the control group without PtNPs treatments. The time taken for wound healing in control i.e., without NP applied on the wound was + 6 h. However, when the wound was covered with the PtNPs paste, it takes only 3 to 4 h for a complete wound healing (Fig. 7). From the SEM analysis of the wound site, it was found that the wound in non-treatment

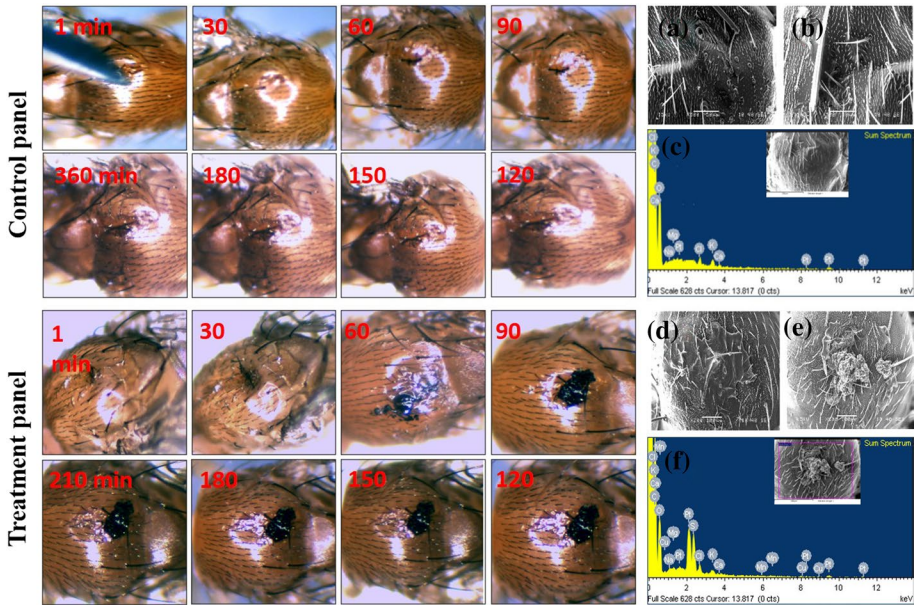

Fig. 7 Wound healing of adult fly; **a**, **b** SEM images of the non-treatment wound; **c** EDX and percentage of hemocyte's element analysis of non-treatment wound; **d**, **e** SEM images of PtNPs paste treatment wound; **f** EDX and percentage of hemocyte's element analysis of PtNPs treatment wound

groups causes necrosis and also damages the neighboring cells (Fig. 7a-b). In PtNP treated flies, the wound healing site does not develop necrosis as found from EDX analysis of the wound (Fig. 7d-e). Since, it was known that the hemolymph possesses many ions and elements such as Na^+, K^+, Cl^-, Ca^{2+}, Mn^{2+}, and Mg^{2+}, the elemental analysis was performed in the wounded site and the weight percentage of the elements was found to be for Na^+ (0.17%), K^+ (0.30%), Cl^- (1.02%), Ca^{2+} (0.34%), Mn^{2+} (0%), and Mg^{2+} (0.06%) respectively for the non-treated wound site (Fig. 7C). For the PtNPs treatment wound it was found to be Na^+ (0.29%), K^+ (0.78%), Cl^- (0.79%), Ca^{2+} (0.42%), Mn^{2+} (0.27%), Pt (22.24%), and Mg^{2+} (0.15%) (Fig. 7f). All ionic percentage increases at the PtNPs treatment site and enhances the rapid angiogenesis and helps in wound healing.

Wound Healing Analysis

From the wound healing activities, it was found that the actin filaments were more active at the initial stage of wound healing. When the wound gets fully healed, then the actin dynamic also gets minimized. It was seen that, in PtNPs treatment groups, the wound site heal around 38% at an initial time period of 1 min and it was reached maxima at 120 min, and then it retarded subsequently with respect to time. At a time point of 180 min, the wound heal completely (Fig. 8c). Whereas in the control untreated group, the wound remain unhealed up to 360 min. Briefly, from the kymograph study, revealed that the actin molecules (indicating as deep red color) have more active on PtNPs applied wound area (Fig. 8c). It was also clearly seen on kymograph analysis that the movement of actin molecules was more in PtNP treated wound area (Fig. 8b,d) initially which become stabilised at later part.

Wound Closure Measurements

Wound closure measurements are the more dynamic method to know the rate and percentage of wound healing with respect to time. From this measurement it was found that the percentage of wound closure was more on PtNPs treatment as compared with the control non-treated ones. At the initial stage the wound (approx. area of wound > 0.06 mm^2) was considered as 100%, and as time increases, the wound started to heal. At 1 min of healing, 8% and 14% of wound healing for control, and PtNPs were applied wound respectively ($P < 0.01$). After 30 min, it was seen that the wound healing in the treatment group was faster as compared to the non-treated control (60% and 32% respectively, $P < 0.001$). The wound of the control group was seen not healed fully until 360 min after wound development (Fig. 8c).

Discussion

The current study established the potentiality of PtNPs as non-cytotoxic and non-genotoxic nanoparticles in the model organism *D. melanogaster*. The study further establishes that PtNPs can induce angiogenesis to aid the wound healing process and can scavenge the ROS in *D. melanogaster*.

From the histological staining, DAPI reveals negligible DNA damage. This study is in agreement with the earlier studies which show PtNPs can also be used in the treatment of cancer cells [13, 45, 46]. Earlier reports of in vitro

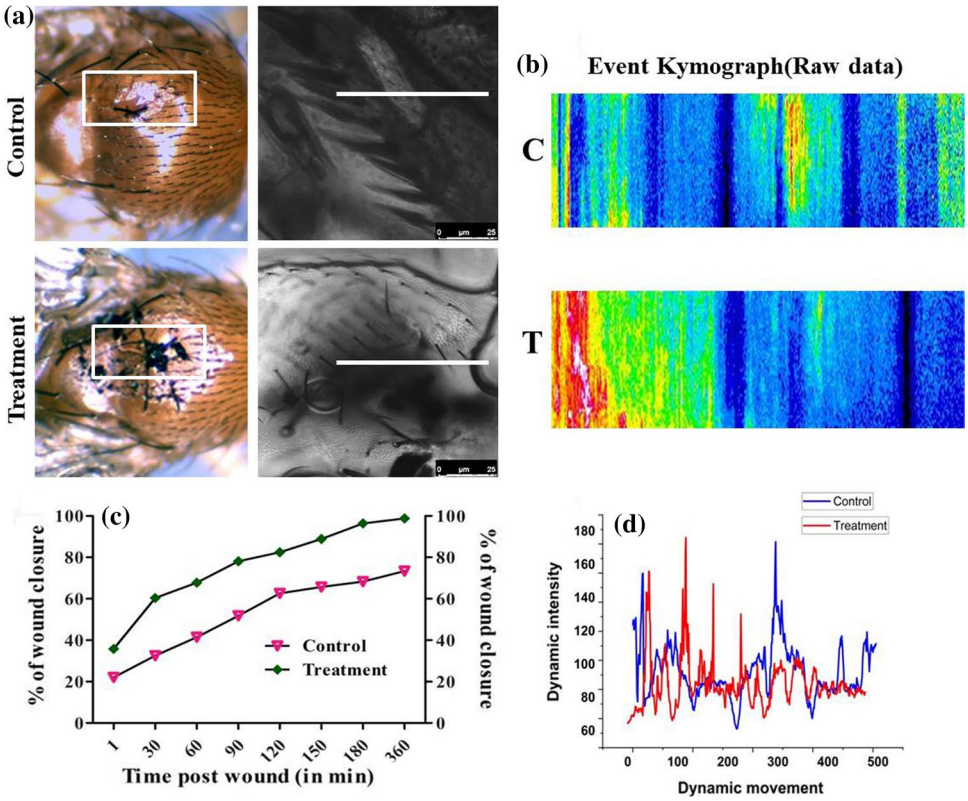

Fig. 8 Wound healing and wound closure analysis of adult fly; **a** PtNPs applied wound under a stereo microscope and confocal microscope; **b** raw data of event kymograph showing the rate of actin molecule movement; **c** graphical representation of the percentage of wound closure rate w.r.t time; **d** graph showed the dynamic intensity of actin movement obtained from kymograph

and in vivo studies showed that PtNPs help in quenching the oxides and hydroxide radicals [10, 47, 48]. Our finding also agreed less production of ROS after PtNPs treatment as evidenced by DCFHDA staining. NBT assay reveals the concentration of superoxide radicals present within the body. The current study evidenced less amount of superoxide radical formation after PtNPs treatment and acts as an antioxidant (Fig S1). The mechanism for ROS scavenging was schematized in supplementary figure (Fig S4).

Further, trypan blue staining showed no internal gut damage and proved PtNPs to be non-toxic. Again, it was worthy to study the interaction of PtNPs and hemocytes. This experiment showed the PtNPs interact with the hemocytes without causing any damage to the hemocytes, besides it can induce the phagocytic cell i.e., plasmatocytes in great number to invade and fight with the foreign particles (Fig. S2).

Mitochondria amount and protein vary according to different nanoparticles. A comparative study of mitochondrial number and mitochondrial protein revealed the details of the induced property of PtNPs. Mitochondria amount altered in many diseased conditions such as diabetes [49], muscular dystrophy [50], and ischemic damage [51]. The NPs such as Au [52, 53], CuO [54], Fe@AuO [55], TiO_2 [56], ZnO [57], and amorphous silica NPs [58] induced ROS in cells, and thus mitochondrial number decreases or down-regulate or dysfunction. However, when cells need high energy, mitochondria number increases i.e., power-hungry cells have more mitochondria than the cells with lower energy needs. Some of the NPs such as PLGA-PEG NPs [59], Dibenzoazepine-PLGA NPs[60], *Momordica charantia* NPs [61], silver NPs and Curcumin NPs [62–64] act as antioxidants and help in the reduction of ROS and also increased the number of mitochondria by promoting the Nrf2 signaling pathway and PGC-1α gene. Our findings also agree with the above statement that mitochondria number and protein concentration can be increased due to the stress level of cells. Our finding is in agreement with this statement that, mitochondrial biogenesis occurs when cells need more energy to overcome from necessity. Therefore, at initial stage, more ROS amount was observed so to overcome mitochondrial biogenesis was marked. This was due to when the larvae get molts into 1st instar, 2nd instar, and 3rd instar, and get metamorphosis on pupa stage to acquire adult. Whole gut was degenerated during metamorphosis and new young gut was developed. In this process, the accumulated NPs assimilated throughout the body and mixed with hemolymph. Thus, at initial stage adult flies shows more ROS production. To overcome from this more amount of mitochondrial biogenesis occurs as well as protein content was also increased. But, later on ROS amount was reduced due to the positive effect of PtNPs inside the cells which act as an antioxidant agent without hindering the hemolymph as well as mitochondria. All these findings suggest that

PtNPs can reduce the ROS level of the cells and increase the biogenesis of mitochondria. In agreement with these results, we also found an increased number of mitochondria after PtNPs treatment.

Although nanoparticles are widely used, genotoxic reports are also coming up from various animal studies. The toxicity of several nanoparticles was reported from the study of *D. melanogaster* [29, 65, 66]. The toxicity of noble metallic nanoparticles like gold and silver were reported in this organism [28, 67]. In the meantime, polymeric nanoparticles like guargum were also reported to be nontoxic in *D. melanogaster* [2]. The PtNPs also did not produce any phenotypic defect after oral treatment. This suggests PtNPs is non-genotoxic in *D. melanogaster* and can be used for future biomedical applications.

Nanoparticles interact with the blood once it is circulated within the hemolymph. Wang et al., 2013 reported that the concentration of hemoglobin and percentage of red blood cells increased in rats treated with graphene quantum dots [68]. The erythrocytes do not show any damage immediately when exposed to toxic substances, because it has an improved antioxidant defense system which includes enzymatic antioxidants such as catalase and peroxiredoxin-2 and nonenzymatic antioxidant as glutathione [69, 70]. The interaction of NPs with blood was also reported by many researchers by in vitro studies [71–74]. PtNPs help in scavenging the intracellular ROS as reported from in vivo study [8, 48, 75, 76]. The nanoparticles such as AgNPs [77], AuNPs [78], and fibrin-based scaffolds containing PLGA [79], were used for wound healing and regeneration. Notably, our finding also suggested that the noble PtNP helps in wound healing. The synthesized PtNPs promisingly help in fastening the wound healing in vivo via inducing the angiogenesis process. However, the percentage occurrence of Cl^- ions in treatment groups is low due to less binding efficacy of Pt towards the Cl^- ions and formed PtCl. This will be helpfull in the development of potential biomedicines to cure accidental wounds.

In summary, our current findings suggest that PtNPs may be potentially effective in protecting against ROS, by scavenging ROS under stress conditions. PtNPs also showed promising findings towards wound healing and angiogenesis. Furthermore, the PtNPs doesnot damage the hemocytes; however, they can promote the plasmatocytes production to help in the defense mechanism. The PtNPs do not show any phenotypic defects in adult flies too. All these findings showed that PtNPs can be used as a potentially important nanoparticle for future biomedical applications; however, due to many contradictory findings regarding PtNPs, a suitable concentration of PtNPs can be used for a better result.

Supplementary Information The online version contains supplementary material available at https://doi.org/10.1007/s10876-022-02292-9.

Acknowledgements JB is thankful to DBT (Grant No. BT/PR21857/NNT/28/1238/2017) for financial support. SM is thankful to MHRD for financial support. MM lab is supported by DBT Grant No. BT/PR21857/NNT/28/1238/2017, Odisha DBT 3325/ST (BIO)-02/2017, and EMR/2017/003054. Dr. Carmel Coelho, Centre for Human Genetics, Bangaluru for providing *UAS-mCD8GFP* fly line.

Author Contributions JB: formal analysis, investigation, writing original draft, data curation; SM: investigation, data curation; MT: investigation, data curation; RM: investigation, data curation; PKS: investigation, data curation; GH: conceptualization, writing review and editing; MM: conceptualization, writing review and editing, supervision, visualization, project administration, funding acquisition, resources.

Availability of data and material All data and material regarding this work are completely transparent.

Declarations

Conflict of Interest The authors have no conflict of interest.

References

1. B. K. Barik and M. Mishra (2019). *Nanotoxicology* **13**, 2.
2. J. Bag, S. Mukherjee, S. K. Ghosh, A. Das, A. Mukherjee, J. K. Sahoo, K. S. Tung, H. Sahoo, and M. Mishra (2020). *Int. J. Biol. Macromol.* **165**, 333.
3. J. Venkatesan, P. K. Gupta, S. E. Son, W. Hur, and G. H. Seong (2022). *J Clust Sci*. https://doi.org/10.1007/s10876-021-02212-3.
4. Y. Jin, B. Li, K. Saravanakumar, X. Hu, and M.-H. Wang (2021). *J Clust Sci*. https://doi.org/10.1007/s10876-021-02024-5.
5. P. K. Mishra, A. Ekielski, S. Mukherjee, S. Sahu, S. Chowdhury, M. Mishra, S. Talegaonkar, L. Siddiqui, and H. Mishra (2019). *Biomolecules* **9**, 8.
6. G. Dhar, S. Mukherjee, N. Nayak, S. Sahu, J. Bag, R. Rout, and M. Mishra. (2020). pp. 223–251. https://doi.org/10.1007/978-1-4939-9756-5_18.
7. T. Mallick, A. Karmakar, J. Bag, S. Sahu, M. Mishra, and N. A. Begum (2020). *Dyes Pigm.* **173**, 107994.
8. A. Watanabe, M. Kajita, J. Kim, A. Kanayama, K. Takahashi, T. Mashino, and Y. Miyamoto (2009). *Nanotechnology* **20**, 45.
9. M. Jeyaraj, S. Gurunathan, M. Qasim, M.-H. Kang, and J.-H. Kim (2019). *Nanomaterials* **9**, 12.
10. S. Shibuya, Y. Ozawa, K. Watanabe, N. Izuo, T. Toda, K. Yokote, and T. Shimizu (2014). *PLoS ONE* **9**, 10.
11. F. Gatto, M. Moglianetti, P. P. Pompa, and G. Bardi (2018). *Nanomaterials* **8**, 6.
12. M. Kutwin, E. Sawosz, S. Jaworski, M. Wierzbicki, B. Strojny, M. Grodzik, M. Ewa Sosnowska, M. Trzaskowski, and A. Chwalibog (2019). *Materials* **12**, 6.
13. J. Depciuch, M. Stec, B. Klebowski, A. Maximenko, E. Drzymała, J. Baran, and M. Parlinska-Wojtan (2020). *Photodiagnosis Photodyn Ther*. https://doi.org/10.1016/j.pdpdt.2019.101594.
14. J. Pelka, H. Gehrke, M. Esselen, M. Türk, M. Crone, S. Bräse, T. Muller, H. Blank, W. Send, and V. Zibat (2009). *Chem. Res. Toxicol.* **22**, 4.
15. T. Hamasaki, T. Kashiwagi, T. Imada, N. Nakamichi, S. Aramaki, K. Toh, S. Morisawa, H. Shimakoshi, Y. Hisaeda, and S. Shirahata (2008). *Langmuir* **24**, 14.
16. T. T. Loan, L. T. Do, and H. Yoo (2018). *J. Nanosci. Nanotechnol.* **18**, 2.

17. H. Gehrke, J. Pelka, C. G. Hartinger, H. Blank, F. Bleimund, R. Schneider, D. Gerthsen, S. Bräse, M. Crone, and M. Türk (2011). *Arch. Toxicol.* **85**, 7.
18. I.A. Shurygina and M.G. Shurygin. (Springer, 2017). pp. 21–37. https://doi.org/10.1007/978-3-319-63790-7_2.
19. M. Yamada, M. Foote, and T. W. Prow (2015). *Wiley Interdiscip. Rev. Nanomed. Nanobiotechnol.* **7**, 3.
20. I. Jung, T.-Y. Kim, and J. Kim-Ha (2011). *FEBS Lett.* **585**, 12.
21. L.-R. Shen, F. Xiao, P. Yuan, Y. Chen, Q.-K. Gao, L. D. Parnell, M. Meydani, J. M. Ordovas, D. Li, and C.-Q. Lai (2013). *Age* **35**, 4.
22. L. N. Lewis and N. Lewis (1986). *J. Am. Chem. Soc.* **108**, 23.
23. N. Toshima and T. Yonezawa (1998). *New J. Chem.* **22**, 11.
24. S. Ishizuka, (1956). In Japanese.
25. Y. Yoshihisa, Q.-L. Zhao, M. A. Hassan, Z.-L. Wei, M. Furuichi, Y. Miyamoto, T. Kondo, and T. Shimizu (2011). *Free Radic. Res.* **45**, 3.
26. Y. Sakaue, J. Kim, and Y. Miyamoto (2010). *Int. J. Nanomed.* **5**, 687.
27. S. A. Pappus and M. Mishra (2018). *Adv Exp Med Biol*. https://doi.org/10.1007/978-3-319-72041-8_18.
28. P. P. Pompa, G. Vecchio, A. Galeone, V. Brunetti, S. Sabella, G. Maiorano, A. Falqui, G. Bertoni, and R. Cingolani (2011). *Nano Res.* **4**, 4.
29. R. Posgai, C. B. Cipolla-McCulloch, K. R. Murphy, S. M. Hussain, J. J. Rowe, and M. G. Nielsen (2011). *Chemosphere* **85**, 1.
30. E. Baeg, K. Sooklert, and A. Sereemaspun (2018). *Nanomaterials* **8**, 10.
31. W. Ji, W. Qi, S. Tang, H. Peng, and S. Li (2015). *Nanomaterials* **5**, 4.
32. S. Priyadarsini, S. Mukherjee, and M. Mishra. (Springer, 2020). pp. 51–64. https://doi.org/10.1007/978-1-4939-9756-5_5.
33. J. Bag and M. Mishra. (Springer, 2020). pp. 151–168. https://doi.org/10.1007/978-1-4939-9756-5_13.
34. N. Nayak and M. Mishra. (Springer, 2020). pp. 123–134. https://doi.org/10.1007/978-1-4939-9756-5_11.
35. S. Alsford, T. Kawahara, C. Isamah, and D. Horn (2007). *Mol. Microbiol.* **63**, 3.
36. G. Dhar, J. Bag, and M. Mishra (2020). *Environ. Sci. Pollut. Res.* **27**, 26.
37. T. Brandt, A. Mourier, L. S. Tain, L. Partridge, N.-G. Larsson, and W. Kühlbrandt (2017). *Elife*. https://doi.org/10.7554/eLife.24662.
38. O. H. Lowry, N. J. Rosebrough, A. L. Farr, and R. J. Randall (1951). *J Biol Chem*. https://doi.org/10.1016/S0021-9258(19)52451-6.
39. J. Bag and M. Mishra. (Springer, 2020). pp. 31–38. https://doi.org/10.1007/978-1-4939-9756-5_3.
40. M. Subalakshmi, A. Saranya, M. U. Maheswari, A. Jarina, and S. Kaviman (2014). *Int. J. Exp. Pharmacol.* **4**, 2.
41. W. Demilew, G. M. Adinew, and S. Asrade (2018). *Evid-Based Complement Altern Med*. https://doi.org/10.1155/2018/2047896.
42. A. Singh and K. Miyabayashi (2020). *RSC Adv.* **10**, 1.
43. K. M. Koczkur, S. Mourdikoudis, L. Polavarapu, and S. E. Skrabalak (2015). *Dalton Trans* **44**, 41.
44. H. Liu, B. Zhang, H. Shi, Y. Tang, K. Jiao, and X. Fu (2008). *J. Mater. Chem.* **18**, 22.
45. A. Aygun, F. Gülbagca, L.Y. Ozer, B. Ustaoglu, Y.C. Altunoglu, M.C. Baloglu, M.N. Atalar, M.H. Alma, and F. Sen (2020). *J. Pharm. Biomed. Anal.* **179**.
46. E. Porcel, S. Liehn, H. Remita, N. Usami, K. Kobayashi, Y. Furusawa, C. Le Sech, and S. Lacombe (2010). *Nanotechnology* **21**, 8.
47. J. Kim, M. Takahashi, T. Shimizu, T. Shirasawa, M. Kajita, A. Kanayama, and Y. Miyamoto (2008). *Mech. Ageing Dev.* **129**, 6.
48. F. Yusof and N. A. S. Ismail (2015). *J. Appl. Pharm. Sci.* **5**, 7.
49. H.-F. Jheng, P.-J. Tsai, S.-M. Guo, L.-H. Kuo, C.-S. Chang, I.-J. Su, C.-R. Chang, and Y.-S. Tsai (2012). *Mol. Cell. Biol.* **32**, 2.
50. P. Grumati, L. Coletto, P. Sabatelli, M. Cescon, A. Angelin, E. Bertaggia, B. Blaauw, A. Urciuolo, T. Tiepolo, and L. Merlini (2010). *Nat. Med.* **16**, 11.
51. E. T. Chouchani, V. R. Pell, E. Gaude, D. Aksentijević, S. Y. Sundier, E. L. Robb, A. Logan, S. M. Nadtochiy, E. N. Ord, and A. C. Smith (2014). *Nature* **515**, 7527.
52. Ö. F. Karataş, E. Sezgin, Ö. Aydın, and M. Culha (2009). *Colloids Surf. B* **71**, 2.
53. M. Mkandawire, M. Lakatos, A. Springer, A. Clemens, D. Appelhans, U. Krause-Buchholz, W. Pompe, G. Rödel, and M. Mkandawire (2015). *Nanoscale* **7**, 24.
54. M. A. Siddiqui, H. A. Alhadlaq, J. Ahmad, A. A. Al-Khedhairy, J. Musarrat, and M. Ahamed (2013). *PLoS ONE* **8**, 8.
55. Y.-N. Wu, L.-X. Yang, X.-Y. Shi, I.-C. Li, J. M. Biazik, K. R. Ratinac, D.-H. Chen, P. Thordarson, D.-B. Shieh, and F. Braet (2011). *Biomaterials* **32**, 20.
56. V. Freyre-Fonseca, N. L. Delgado-Buenrostro, E. B. Gutiérrez-Cirlos, C. M. Calderón-Torres, T. Cabellos-Avelar, Y. Sánchez-Pérez, E. Pinzón, I. Torres, E. Molina-Jijón, and C. Zazueta (2011). *Toxicol. Lett.* **202**, 2.
57. V. Sharma, D. Anderson, and A. Dhawan (2012). *Apoptosis* **17**, 8.
58. L. Sun, Y. Li, X. Liu, M. Jin, L. Zhang, Z. Du, C. Guo, P. Huang, and Z. Sun (2011). *Toxicol. In Vitro* **25**, 8.
59. E. L. Vallorz, K. Blohm-Mangone, R. G. Schnellmann, and H. M. Mansour (2021). *AAPS J* **23**, 4. https://doi.org/10.1208/s12248-021-00619-4.
60. D. Huang, N. Narayanan, M. A. Cano-Vega, Z. Jia, K. M. Ajuwon, S. Kuang, and M. Deng (2020). *Iscience* **23**, 6. https://doi.org/10.1016/j.isci.2020.101167.
61. O. O. Elekofehinti, O. C. Ayodele, and O. Iwaloye (2021). *Egypt. J. Med. Hum. Genet.* **22**, 1.
62. M. R. de Oliveira, F. R. Jardim, W. N. Setzer, S. M. Nabavi, and S. F. Nabavi (2016). *Biotechnol. Adv.* **34**, 5.
63. J. Lone, J. H. Choi, S. W. Kim, and J. W. Yun (2016). *J Nutr Biochem*. https://doi.org/10.1016/j.jnutbio.2015.09.006.
64. M. Negrette-Guzmán, W.R. García-Niño, E. Tapia, C. Zazueta, S. Huerta-Yepez, J.C. León-Contreras, R. Hernández-Pando, O.E. Aparicio-Trejo, M. Madero, and J. Pedraza-Chaverri (2015). *Evid. Based Complement. Altern. Med*. https://doi.org/10.1155/2015/917435.
65. S. A. Pappus, B. Ekka, S. Sahu, D. Sabat, P. Dash, and M. Mishra (2017). *J. Nanoparticle Res.* **19**, 4.
66. K. Sood, J. Kaur, H. Singh, S. K. Arya, and M. Khatri (2019). *Toxicol Rep*. https://doi.org/10.1016/j.toxrep.2019.07.009.
67. E. Demir, G. Vales, B. Kaya, A. Creus, and R. Marcos (2011). *Nanotoxicology* **5**, 3. https://doi.org/10.3109/17435390.2010.529176.
68. K. Wang, Z. Gao, G. Gao, Y. Wo, Y. Wang, G. Shen, and D. Cui (2013). *Nanoscale Res. Lett.* **8**, 1.
69. R. Gonzales, C. Auclair, E. Voisin, H. Gautero, D. Dhermy, and P. Boivin (1984). *Cancer Res.* **44**, 9.
70. K.-K.L. Shin, S.G. Rhee, and D.-Y. Yu. *Blood* **101**, 12
71. C. Fornaguera, G. Calderó, M. Mitjans, M. P. Vinardell, C. Solans, and C. Vauthier (2015). *Nanoscale* **7**, 14.
72. A. N. Ilinskaya and M. A. Dobrovolskaia (2016). *Front Nanobiomed Res*. https://doi.org/10.1142/9789813140455_0008.
73. F. Esmaeili, M. H. Ghahremani, B. Esmaeili, M. R. Khoshayand, F. Atyabi, and R. Dinarvand (2008). *Int J Pharm* **349**, 1.
74. G. G. De La Cruz, P. Rodríguez-Fragoso, J. Reyes-Esparza, A. Rodríguez-López, R. Gómez-Cansino, and L. Rodriguez-Fragoso (2018). *Unraveling the Safety Profile of Nanoscale Particles and Materials-From Biomedical to Environmental Applications*. https://doi.org/10.5772/intechopen.69386.
75. A. Anju, K. Gupta, and T. S. Chundawat (2020). *Turk. J. Pharm. Sci.* **17**, 3.

76. P. Jawaid, M. U. Rehman, M. A. Hassan, Q. L. Zhao, P. Li, Y. Miyamoto, M. Misawa, R. Ogawa, T. Shimizu, and T. Kondo (2016). *Ultrason. Sonochem.* **31**, 206.
77. C. Rigo, L. Ferroni, I. Tocco, M. Roman, I. Munivrana, C. Gardin, W. R. Cairns, V. Vindigni, B. Azzena, and C. Barbante (2013). *Int. J. Mol. Sci.* **14**, 3.
78. J.-G. Leu, S.-A. Chen, H.-M. Chen, W.-M. Wu, C.-F. Hung, Y.-D. Yao, C.-S. Tu, and Y.-J. Liang (2012). *Nanomedicine* **8**, 5.
79. A. E. Krausz, B. L. Adler, V. Cabral, M. Navati, J. Doerner, R. A. Charafeddine, D. Chandra, H. Liang, L. Gunther, and A. Clendaniel (2015). *Nanomedicine* **11**, 1.

Authors and Affiliations

Janmejaya Bag[1] · Sumit Mukherjee[1] · Manamohan Tripathy[2] · Rudramadhab Mohanty[1] · Pranab Kumar Shendha[1] · Garudadhwaj Hota[2] · Monalisa Mishra[1]

✉ Monalisa Mishra
mishramo@nitrkl.ac.in

[1] Neural Developmental Biology Lab, Department of Life Science, National Institute of Technology, Rourkela, Odisha 769008, India

[2] Department of Chemistry, National Institute of Technology, Rourkela, Odisha 769008, India